4.8 A Terahertz FMCW Comb Radar in 65nm CMOS with 100GHz Bandwidth

Xiang Yi[1], Cheng Wang[1], Muting Lu[1], Jinchen Wang[1], Jesus Grajal[1,2], Ruonan Han[1]

[1]Massachusetts Institute of Technology, Cambridge, MA
[2]Universidad Politécnica de Madrid, Madrid, Spain

The increasing demands for low-cost, compact, and high-resolution radar systems have driven the operation frequency to terahertz (THz) due to the shorter wavelength and larger bandwidth [1-5]. However, conventional single-transceiver FMCW radar chips only provide limited signal bandwidth (<70GHz [1-5]), especially when implemented using CMOS technologies with low f_T and f_{max}. Therefore, prior THz integrated radars are based on compound semiconductors [2-4] and have severely degraded performance near the band edges. That not only limits their applications in high-accuracy scenarios like industrial robotics and small-defect detections, but also poses tradeoffs between bandwidth and detection range. To break such limitations, this paper adopts a frequency-comb-based scalable architecture using a paralleled transceiver array to cover an ultra-broad bandwidth. Implemented in a 65nm bulk CMOS process, a five-transceiver radar chip is prototyped with seamless coverage of the entire 220-to-320GHz band and a ranging resolution of 1.5mm. Across the state-of-the-art total chirp bandwidth of 100GHz, the output power fluctuates by only 8.8dB.

The concept of the FMCW comb radar is illustrated in Fig. 4.8.1, where a 100GHz bandwidth (*BW*) is divided into *N* segments with identical bandwidths of 20GHz (*BW/N)*. These segments are swept simultaneously using an array of transceivers (i.e. channels) with equally-spaced carrier frequencies (i.e. comb). Each transceiver has its own antenna, and the received echo signal is mixed with the transmitted signal to generate an IF output. According to Fig. 4.8.1, the phase of the IF output of a certain channel is independent of the absolute phase of the related TX signal (φ_N). Meanwhile, a critical observation is that with identical chirp length ΔT among all channels, the endpoint's phase of the IF signal in one certain channel well matches the starting-point's phase of the IF signal in the next channel. That means a direct stitching of the time-domain IF signals after the standard chirp-nonlinearity calibration incurs negligible phase discontinuity and the result emulates the IF signal of an equivalent broadband (*BW*) radar. Lastly, it also allows for the daisy-chain architecture presented in Fig. 4.8.1, since there is no need for calibrating the accumulated TX phase mismatch along the chain. In this architecture, a 13.75-to-15GHz external FMCW signal with 25% over-chirping (to ensure the frequency continuity between adjacent channels) is fed at the left end of the chain, frequency-multiplied by 4, and then upconverted successively with a conversion step of 5GHz. The generated signal at each stage is used as the driver signal of the THz transceiver (TRX) in the associated channel. The presented high-parallelism scheme offers several advantages over single-transceiver radars. Firstly, scalable bandwidth extension is achieved and enables implementations in less advanced technologies (e.g. 65nm CMOS) as well as flatter frequency responses across the entire operation band [6]. Secondly, the flat frequency response also leads to higher linearity of the equivalent chirp signal (hence reduced linewidth broadening after FFT) [7]. Thirdly, given a certain chirp slope, the duration of each equivalent broadband ($N{\cdot}\Delta B$) sweep is reduced by *N*. The *SNR* of the comb radar is therefore improved by *N* for a given total detection time.

The schematics of the THz transmitter and receiver are shown in Fig. 4.8.2. First, the millimeter-wave input FMCW chirp signal is frequency-doubled and then fed into a folded slot balun [6]. The balun has a simulated insertion loss of 1.3dB and an amplitude/phase mismatch of 0.05dB/0.5° within the 10GHz bandwidth; the latter is critical to the succeeding pseudo-differential amplifier chain, which is highly sensitive to input imbalance. The transformer-coupled amplifier with neutralization drives Doubler 2 with saturated output power. For the transmission mode, the THz output signal feeds into the antenna through a multi-stub matching network with 1-to-1.5dB insertion loss. Note that a single-antenna solution is adopted for its compactness, which is critical to the comb radar architecture. Part of the TX signal is also combined with the radar echo signal received by the antenna and then flows into a passive-mixer-first THz receiver (Fig. 4.8.2). Such a receiver structure offers low flicker noise and excellent linearity. The latter, combined with the fact that the TX signal is directly used as the mixer LO, eliminates the TX-RX leakage problem in conventional radars with LNAs. Any unwanted low-frequency RX IF signal, due to reflections at nearby objects (e.g. bond wires) and due to power fluctuation of the THz LO signal during chirping, is suppressed by an *RC* highpass filter. Lastly, the IF signal is boosted by a self-biased, two-stage LNA with 3.3nV/√Hz simulated input-referred noise, and is then processed by an off-chip amplifier and a digitizer. Between channels, the frequency conversion is realized by an SSB mixer, of which the RF IQ signals are generated by a broadband, compact *RC* polyphase filter. The 5GHz mixer IQ LO signals are from a divider (÷2) clocked at 10GHz.

To avoid the costly silicon lens used in [2,4], THz antennas with front-side radiation are preferred. Conventional patch antennas [3] avoid the lossy substrate waves at THz, but fail to provide flat response over the required 20GHz channel bandwidth, due to the high-Q resonant mode formed by the closely-spaced top and bottom metal layers. In our chip, a multi-mode substrate-integrated-waveguide (SIW) antenna is adopted, which has two orthogonal slots on a metal cavity (Fig. 4.8.3). The cavity is formed by an aluminum top plane, an M1-M2 stacked bottom plane, and M3-to-M9 stacked sidewalls. To increase the bandwidth, four resonant modes are introduced. Each of their resonant frequencies is jointly determined by the cavity dimensions (W_{cav} and L_{cav}) and the slot length. As such, the two slots with different lengths L_{slot1} and L_{slot2} generate two pairs of resonant modes, of which the resonant frequencies are closely spaced and enable ~40GHz matched bandwidth (Fig. 4.8.3). Our electromagnetic simulation shows that the long slot L_{slot1} radiates at lower frequency, while the short slot L_{slot2} radiates at higher frequency. The polarization direction is frequency dependent, but always linear, which is verified by the >11.6dB simulated axial ratio across the operation band. The simulated antenna gain has a peak value of 0dBi and fluctuates by only 1dB across 20GHz bandwidth. Lastly, the high confinement of the resonance wave in the metal cavity enables low coupling (<-31dB) between adjacent antennas.

The chip was characterized using a VDI Erickson PM5 power meter and a WR3.4 VNA extender. The measured on-chip antenna pattern has a 3dB beamwidth of ~90°. Beyond the far-field distance of ~4cm, the measured TX power-distance dependency well agrees with the Friis equation. The TX EIRP of each channel is shown in Fig. 4.8.4, leading to a multi-channel-aggregated EIRP of 0.6dBm. With a low-cost TPX polymethylpentene lens at the chip front, the above parameter is boosted to ~20dBm. Without the lens, the measured peak RX gain and minimum noise figure (NF), including the baseband amplifier and ~6dB antenna loss, are 22.2dB and 22.8dB, respectively. Thanks to the comb architecture, the fluctuations of the TX power and the RX NF across the 100GHz bandwidth are 8.8dB and 14.6dB, respectively, which well compare with prior broadband THz radars with smaller bandwidth [2,3] (Fig. 4.8.6). To realize ranging detection, the input FMCW chirp signal is generated by a DDS (AD9164-FMCB-EBZ) and a multiplier chain. The five RX outputs are acquired synchronously by a multi-channel digitizer (NI PXI-5105) and then calibrated and stitched in a PC. A set of corner reflectors are measured (Fig. 4.8.5) to verify the aforementioned IF stitching. For instance, Fig. 4.8.5 shows that a single channel *(BW*=20GHz) is unable to resolve two reflectors with 2.5mm range difference. With the stitching of three adjacent channels (*BW*=60GHz), the separation of the objects starts to show. With all five channels stitched together, the separation is distinct. This chip has an area of 5mm^2 and consumes 840mW of power.

Acknowledgements:
The authors would like to thank the TSMC University Shuttle Program for chip fabrication, and thank Qingyu Yang, Nathan Monroe (MIT), Pu Wang, and Rui Ma (Mitsubishi Electric Research Labs) for their help on the measurement. This work is supported by a NSF CAREER award (ECCS-1653100).

References:
[1] B. Ginsburg et al., "A 160GHz Pulsed Radar in 65nm CMOS," *IEEE JSSC.*, vol. 49, no. 4, pp. 984-995, Apr. 2014.
[2] J. Grzyb et al., "A 210–270-GHz Circularly Polarized FMCW Radar with a Single-Lens-Coupled SiGe HBT Chip," *IEEE Trans. THz Sci. Technol.*, vol. 6, no. 6, pp. 771-783, Nov. 2016.
[3] J. Al-Eryani et al., "Fully Integrated Single-Chip 305–375-GHz Transceiver With On-Chip Antennas in SiGe BiCMOS," *IEEE Trans. THz Sci. Technol.*, vol. 8, no. 3, pp. 329-339, May 2018.
[4] A. Mostajeran et al., "A High-Resolution 220-GHz Ultra-Wideband Fully Integrated ISAR Imaging System," *IEEE TMTT,* vol. 67, no. 1, pp. 329-339, Jan. 2019.
[5] A. Visweswaran et al., "A 145GHz FMCW-Radar Transceiver in 28nm CMOS," *ISSCC,* pp. 168-169, Feb. 2019.
[6] C. Wang and R. Han, "Rapid and Energy-Efficient Molecular Sensing Using Dual mm-Wave Combs in 65nm CMOS: A 220-to-320GHz Spectrometer With 5.2mW Radiated Power and 14.6-to-19.5dB Noise Figure," *ISSCC*, pp. 302-303, Feb. 2017.
[7] S. Balon et al., "A C-Band FMCW SAR Transmitter With 2-GHz Bandwidth Using Injection-Locking and Synthetic Bandwidth Techniques," *IEEE TMTT,* vol. 66, no. 11, pp. 5095-5105, Nov. 2018.

 978-1-7281-3205-1/20/$31.00

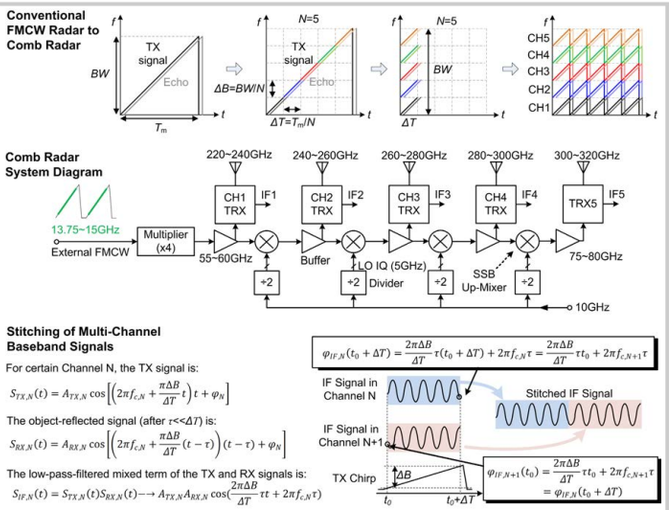

Figure 4.8.1: The basic concept, system diagram and IF signal stitching of the THz comb radar.

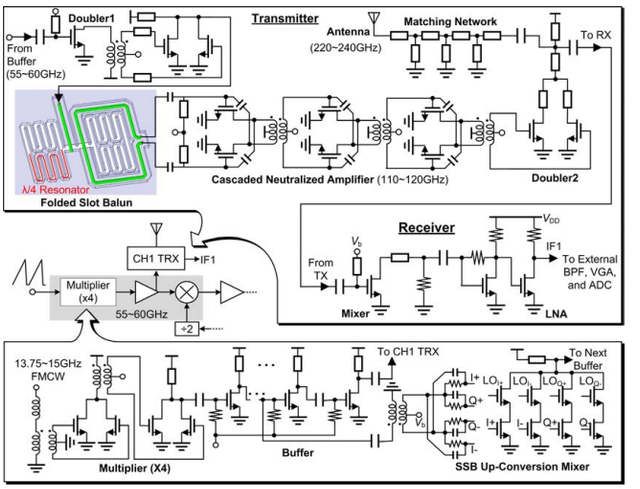

Figure 4.8.2: Schematics of the THz transmitter and receiver of one channel (CH1), as well as the input multiplier, buffer, and SSB upconversion mixer along the frequency-conversion chain.

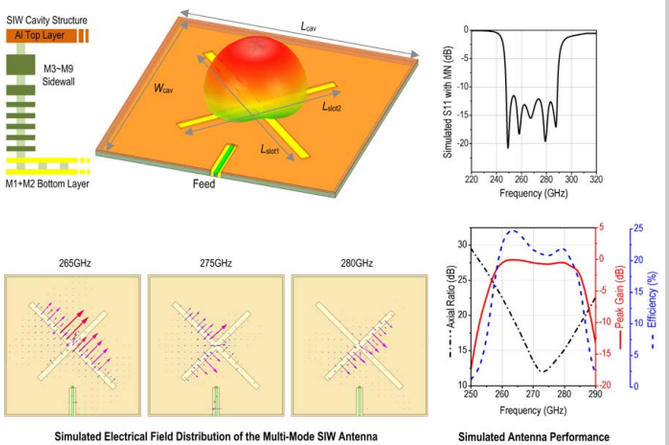

Figure 4.8.3: Structure and simulation of the multimode SIW antenna (CH3).

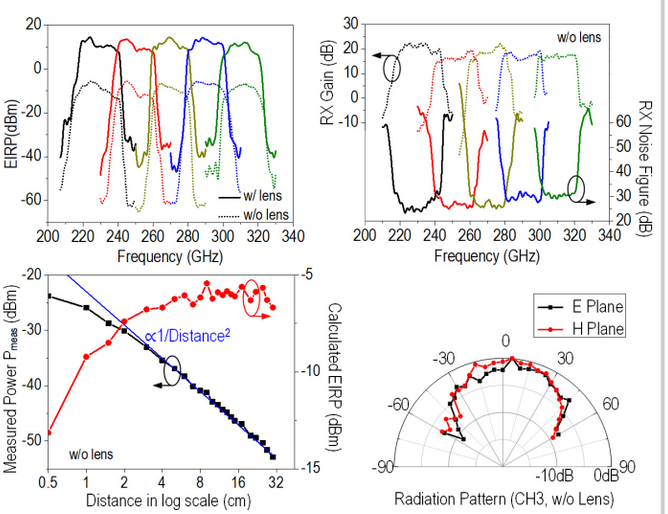

Figure 4.8.4: Measured TX and RX performance of the comb radar chip.

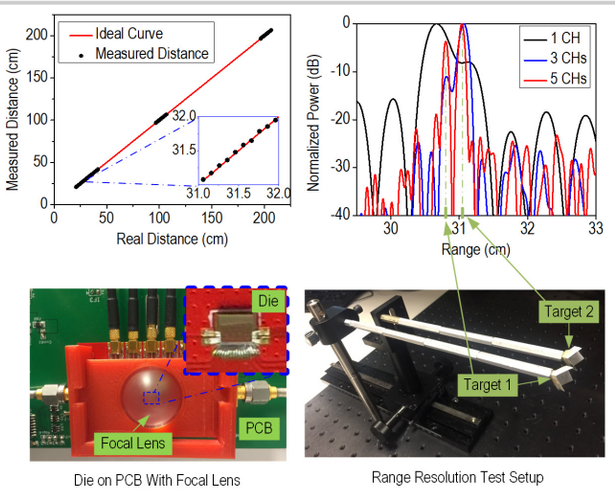

Figure 4.8.5: Measured ranging accuracy and resolution without windowing. Photos of the die on PCB with TPX lens and ranging resolution test setup are also shown.

References	This Work	JSSC 2014 [1]	Trans. THz 2016 [2]	Trans. THz 2018 [3]	T-MTT 2019 [4]	ISSCC 2019 [5]
Technology	65nm CMOS	65nm CMOS	130nm SiGe	130nm SiGe	55nm SiGe	28nm CMOS
Frequency (GHz)	220~320	157.9~164.9	210~270	305~375	189.9~252.3	138~151
Bandwidth (GHz)	100	7	60	70	62.4	13
Resolution (mm)	1.5	21	2.5	2.1	2.4	11.5
Output EIRP (dBm)	0.6, 20[a]	18.8	32.8[b]	6, 18.4[a]	14[b]	11.5
Minimum Noise Figure (dB)	22.2[c]	22.5	21	19.7	NA	4(EINF)[d]
Power/NF Fluctuation (dB)	8.8/14.6	3/NA	20/29	10.5/28.6	7.7/NA	1.5/4
Chip Size (mm^2)	5.0	20	3.2	2.85	0.51	6.5
DC Power (mW)	840	2200	1800	1700	87	500

(a) With TPX focus lens; (b) with silicon lens; (c) includes antenna and baseband; (d) effective isotropic NF which includes the antenna directivity.

Figure 4.8.6: Comparison with state-of-the-art integrated radars.

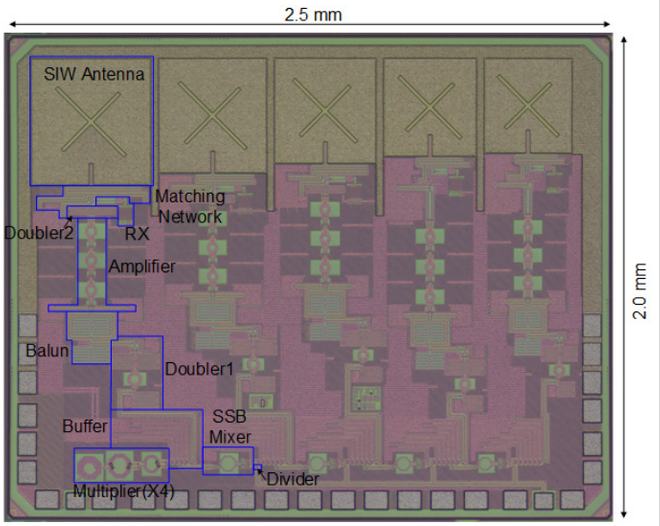

Figure 4.8.7: Die micrograph.

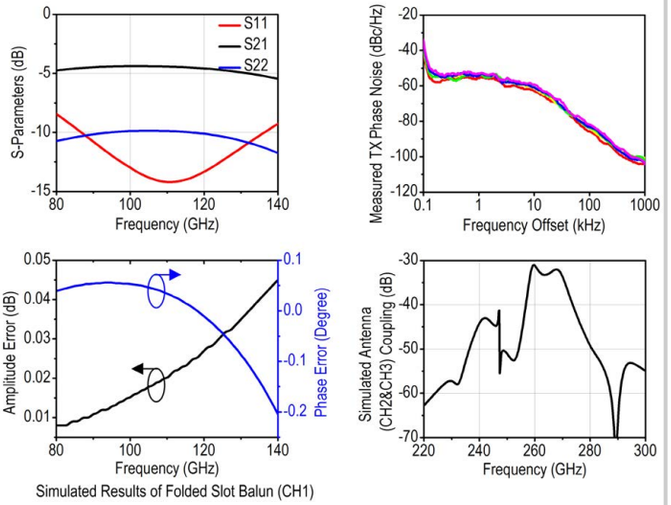

Figure 4.8.S1: Simulated results of folded slot balun (CH1); measured TX phase noise for 5 channels; simulated antenna coupling between CH2 and CH3.

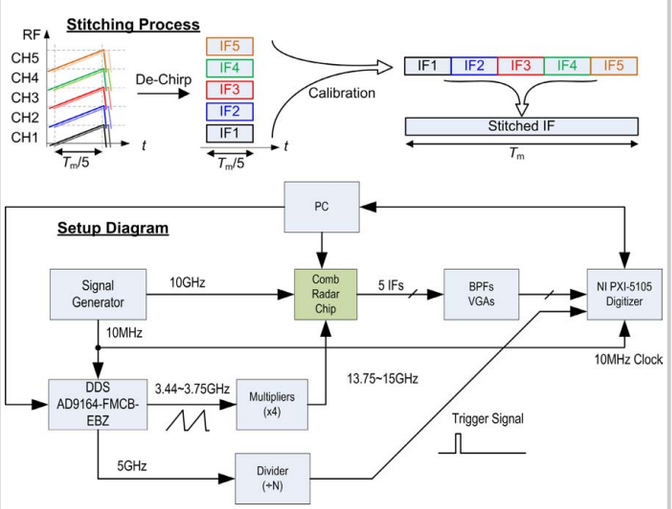

Figure 4.8.S2: IF signal stitching process and setup diagram for FMCW radar ranging accuracy and resolution measurement.

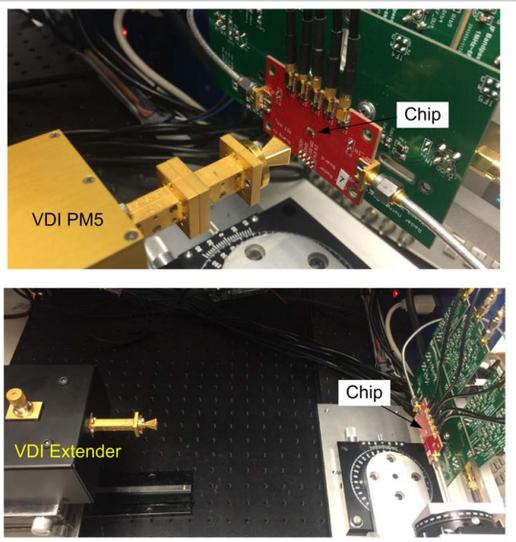

Figure 4.8.S3: Setups for TX and RX measurement without lens.

978-1-7281-3205-1/20/$31.00 ©2020 IEEE